Validation of CFD simulations for X-31 wind-tunnel models

M. Ghoreyshi
Mehdi.Ghoreyshi@usafa.edu
A. D. H. Kim, A. Jirasek, A. J. Lofthouse and R. M. Cummings
High Performance Computing Research Center
US Air Force Academy
Colorado
USA

ABSTRACT

Computational Fluid Dynamics (CFD) has become an attractive method of choice in the design of many aerospace vehicles because of advances in numerical algorithms and convergence acceleration methods. However, the flow around an advanced fighter aircraft is complicated and usually unsteady due to the presence of vortex-dominated flows. The accuracy and predictability of conventional turbulence models for these applications may be questionable and therefore results obtained from these models must be validated and evaluated on the basis of experimental data from wind tunnels and/or flight tests. This work aims to validate CFD simulations of X-31 wind-tunnel models with and without a belly-mounted sting. The sting setup facilitates forced sinusoidal oscillations in one of three modes of: pitch, yaw, and roll. However, the results show that measured aerodynamic data are altered by the turbulent wake behind the sting, even at small angles of attack. The high angle-of-attack flow around the X-31 is also very complicated and unsteady due to canard and wing vortices. Therefore, validation of CFD models for predicting these complex flows can be a very challenging task. The X-31 wind-tunnel experiments were carried out in the German Dutch low-speed wind tunnel at Braunschweig and include aerodynamic force and moment measurement as well as span-wise pressure distributions at locations of 60% and 70% chord length. This data set is used to validate the Cobalt and Kestrel flow solvers and the results are similar and match quiet well with experiments for small to moderate angles of attack. The main discrepancies between CFD and measurements occur close to the wing tip, where leading-edge flaps are located.

Paper No. 4166. Manuscript received 31 March 2014, revised version received 25 September 2014, accepted 2 November 2014.

https://doi.org/10.1017/S0001924000010575 Published online by Cambridge University Press

1.0 INTRODUCTION

The Department of Aeronautics at the US Air Force Academy (USAFA) has a long history of involving cadets in various research programs. All of the cadets in the Aeronautical Engineering major take a course in computational fluid dynamics methods (AE342- Computational Aerodynamics), and then may take an elective course in CFD (AE472 - Advanced CFD)[1]. In addition, highly motivated cadets often take independent research courses with faculty when they are interested in the topic area, which would certainly be true if a significant computational stability and control project was being conducted (AE499- Independent Study). As part of these follow-on courses, the cadets must complete a research project while working with faculty researchers. Some recent research projects include investigation of unsteady flows, boundary layers, turbulence models, shocks, and multi-physics simulations. These projects involve the computational facilities of the department, including the use of DoD's High Performance Computing (HPC) systems. The current paper presents the findings of a cadet research project undertaken in the AE472 course. The objective of this project is to validate CFD simulations for fighter aircraft configurations.

Modern fighter aircraft have become faster and more agile by using sharp leading-edges and highly swept delta wings[2]. Other design features include leading-edge extensions (LEX) and close-coupled canards, in which canard deflections have significant effects on the wing-canard aerodynamic interactions (examples include the NASA X-29 and SAAB Gripen)[3]. Typically, the flow about these aircraft is dominated by the vortices generated on the sharp leading edges of the forebody, LEX, wing, and control surfaces[4]. The interaction between these vortices causes the aerodynamic loads to become strong nonlinear functions of angle-of-attack such that a small change in angle-of-attack can result in large changes in airloads[5]. Furthermore, the airloads depend not only on the current state of flow but also on all the past values of these states. This poses a very difficult challenge for Stability and Control (S&C) analysis of fighter aircraft because the nonlinear and unsteady aerodynamics acting on them cannot be accurately predicted on the basis of stability derivative analysis.

S&C engineers often use an iterative process combining handbook methods, linear aerodynamics assumptions, wind-tunnel testing, and flight test techniques to determine the aerodynamic characteristics of new fighter aircraft. High quality production wind-tunnel testing is expensive since thousands of hours of testing are required at multiple facilities. The wind-tunnel measurements also suffer from scale and interference effects, and are limited in terms of the dynamic motions achievable. Flight tests are even more expensive (an order of magnitude higher than wind-tunnel testing), and usually come very late in the design cycle. The traditional wind-tunnel/flight test approach for determining aircraft aerodynamics is extremely expensive and time consuming. Handbook methods and linear aerodynamics are generally incapable of reliably predicting unsteady nonlinear aerodynamic behavior over the full flight envelope. Furthermore, handbook methods are not accurate for novel configurations. Clearly, a high-fidelity computational tool capable of reliably predicting and/or identifying configurations susceptible to handling quality instabilities prior to flight testing would be of great interest to the S&C community. Such a tool is well suited to the aircraft design phase and would greatly decrease the cost and risks incurred by flight testing and post-design-phase modifications.

The main aerodynamic prediction codes used at USAFA are Cobalt[6] and Kestrel[7], which are hybrid unstructured grid Navier-Stokes flow solvers. Kestrel is a relatively new DoD-developed code; the development started in 2008 as part of the Computational Research and Engineering Acquisition Tools and Environments (CREATE) Program. Both Cobalt and Kestrel originated from the Air Vehicles Unstructured Solver (AVUS, formally known as Cobalt60[8], which is a

https://doi.org/10.1017/S0001924000010575 Published online by Cambridge University Press

parallel, implicit, unstructured flow solver developed by the Air Force Research Laboratory. The computational kernel of Cobalt60[8] is Godunov's first-order accurate, exact Riemann method[9]. Both solvers have since been highly modified. Some turbulence models available in both codes include the Spalart-Allmaras (SA) model, Wilcox's $k - \omega$, Mentor's SST-model, and the SA model with Rotation Correction (SARC). However, since these models are Reynolds Averaged Navier-Stokes (RANS) models, they can only describe the mean flow and would likely fail to accurately predict the unsteady flow effects on aircraft aerodynamic behavior. For the unsteady aerodynamic predictions, the Delayed Detached-Eddy Simulation (DDES) of these turbulence models is also available. However, DDES typically requires many numerical iterations and is more expensive to use.

The X-31 experimental aircraft is a super-maneuverable fighter (a fighter with post-stall maneuvering capability), built by the United States and West Germany in the 1990s. The movable paddles placed in the jet exhaust were used to provide longitudinal and lateral controls at angles of attack well beyond stall. The aircraft incorporates a sharp/leading-edge extension, cranked wing, and a long-coupled canard which deflects between +20 and –70 degrees. In addition to the experimental testing, the X-31 aircraft has been the subject of several CFD simulations[10,11,12]. The X-31 stability and control derivatives were also calculated with CFD and were validated with measurements[13,14].

Schütte *et al*[11] detailed the basic flow topology of the X-31 configurations predicted using the DLR-TAU flow solver using the SA and $k - \omega$ turbulence models. Figure 1 shows that major predicted flow features at 14 degrees angle-of-attack are vortices originating from the wing and control devices. The aerodynamic behaviour of aircraft for angles of attack in the range of 10° and 30° can be explained based on these predicted vortices. In this paper, the predicted vortical flow features of X-31 are described in detail for a range of angles of attack.

The objective of the present paper is to validate CFD models for the complex flow over the challenging X-31 wind-tunnel model geometry and to investigate the effects of turbulence models on the solver predictions. The X-31 aircraft has been considered in this study because the aircraft is an example of a highly agile aircraft with post-stall manoeuvrability and has been the subject of extensive wind-tunnel/flight tests[5,15,16]. Furthermore, the flow around the X-31 is very complicated due to the canard, LEX, and wing vortices. Therefore, validation of CFD models by experimental data can be a very challenging task. The X-31 experimental data are available from the German-Dutch Low-Speed Wind Tunnel at the German Aerospace Center (DLR). These experiments were performed in the framework of the NATO RTO Task Group AVT-161 'Assessment of Stability and Control Prediction Methods for NATO Air & Sea Vehicles', in which both USAFA and DLR participated. In the experimental setup, the wind-tunnel model was mounted on a belly sting that allows forced sinusoidal oscillations in modes of pitch, yaw, and roll. In order to minimise wall effects in dynamic measurements, static measurements were performed in the open as well as the closed test sections. The experimental results show that measured aerodynamic data are altered by the presence of the belly sting, even at small angles of attack[11]. The effects of the belly sting on CFD predictions are also investigated in this paper.

2.0 METHODOLOGY

2.1 Cobalt solver

Cobalt solves the unsteady, three-dimensional, compressible Reynolds-Averaged Navier-Stokes (RANS) equations in an inertial reference frame. The Navier-Stokes equations are discretised on arbitrary grid topologies using a cell-centreed finite volume method. Second-order accuracy

https://doi.org/10.1017/S0001924000010575 Published online by Cambridge University Press

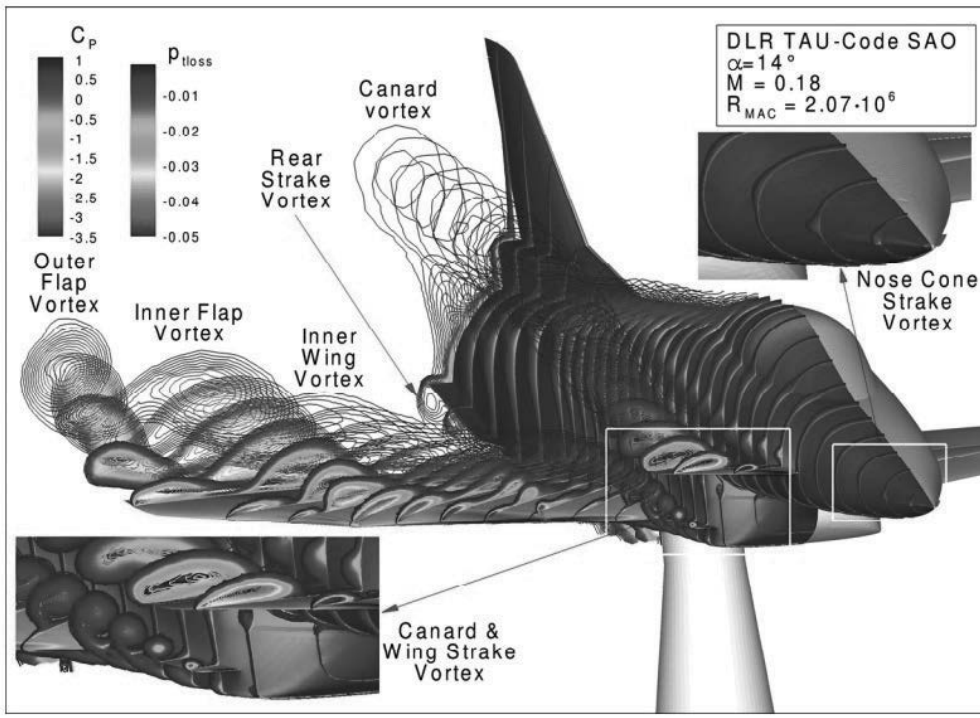


Figure 1. Vortex topology over the X-31 configuration[11].

in space is achieved using the exact Riemann solver of Gottlieb and Groth[8], and least squares gradient calculations using QR factorisation. To accelerate the solution of the discretised system, a point-implicit method using analytic first-order inviscid and viscous Jacobians is implemented. A Newtonian sub-iteration method is used to improve the time accuracy of the point-implicit method. Tomaro *et al*[17] converted the code from explicit to implicit, enabling Courant-Friedrichs-Lewy numbers as high as 10^6. Some available turbulence models are the Spalart-Allmaras model[18], Wilcox's k-ω model[19], and Menter's SST model[20].

2.2 Kestrel Solver

Kestrel is a relatively new DoD-developed CFD solver in the framework of the CREATE Program, which is funded by the High Performance Computing Modernisation Program (HPCMP). The CREATE Program is a 12-year program, started in 2008, and is aimed at addressing the complexity of applying computationally-based engineering to improve DoD acquisition processes[21]. CREATE consists of three computationally-based engineering tool sets for design of air vehicles, ships, and radio-frequency antennae. The fixed-wing analysis code, Kestrel, is part of the Air Vehicles Project (CREATE-AV) and is a modularised, multidisciplinary, virtual aircraft simulation tool incorporating aerodynamics, structural dynamics, kinematics, and kinetics[21].

The flow solver component of Kestrel (kCFD) solves the unsteady, three-dimensional, compressible RANS equations on hybrid unstructured grids[7]. Its foundation is based on Godunov's first-order accurate, exact Riemann solver[9]. Second-order spatial accuracy is obtained through a least squares reconstruction. The code also uses an implicit Newton sub-iteration method to

https://doi.org/10.1017/S0001924000010575 Published online by Cambridge University Press

improve time accuracy. Grismer *et al*[22] parallelised the code, with a demonstrated linear speed-up on thousands of processors. Kestrel receives an eXtensible Markup Language (XML) input file generated by the Kestrel User Interface and stores the solution convergence and volume results in a common data structure for later use by the Output Manager component. Some available turbulence models are the Spalart-Allmaras model, SARC, and DDES with SARC.

2.3 Turbulence modeling

Turbulence modeling refers to replacing Reynolds stress tensor terms in the RANS equations by semi-empirical equations calibrated from experimental data and/or direct numerical simulations. These turbulence models can only approximate the turbulence effects on the mean flow behaviour and do not predict the details of turbulent flow. The most popular methods in turbulence modeling are those that are based on the Boussinesq eddy viscosity approximation which assumes that components of the Reynolds stress tensor are a linear function of the mean velocity gradients such as

$$R_{ij} = \frac{2}{3}k\delta_{ij} - 2\nu_t(S_{ij} - \frac{1}{3}S_{kk}\delta_{ij}) \quad \ldots (1)$$

where δ_{ij} is the Kronecher delta, R_{ij} is the Reynolds stress tensor, S_{ij} is the mean flow strain-rate tensor which is proportional to the mean velocity vector, k is the turbulent kinetic energy per unit mass, and v_t is eddy viscosity. Many formulations of one-equation and two-equation models have been proposed to determine the eddy viscosity in the Boussinesq approximation given in Equation (1), where the accuracy of each model depends on the validity of the simplifying assumptions behind it. In general, the Boussinesq approximation assumes that transport of momentum by turbulence is a diffusive process and therefore it limits models to predict the nondiffusive nature of vortical flows[23].

Turbulence models used in this study include the Spalart-Allmaras (SA) and Spalart-Allmaras with Rotation Correction (SARC) models. The SA model[18] is a popular one-equation model that solves a transport equation for a modified eddy-viscosity coefficient. The SA model can be written in general form as[24]:

$$\frac{D\tilde{\nu}}{Dt} = P + D_{diff} + D_{diss} \quad \ldots (2)$$

where $\tilde{\nu}$ is related to the kinematic eddy viscosity, P is the turbulence due to production, D_{diff} is the turbulence due to gradient of diffusion, and D_{diff} is the near wall dissipation of turbulent kinematic viscosity. The production term is given by;

$$P = C_{b1}(1 - f_{t2})W\tilde{\nu} \quad \ldots (3)$$

where W is the magnitude of vorticity. The SA model has been calibrated using a wide range of experimental data of several well-documented flow cases and has proven to be robust, relatively low cost, and simple because it does not need standard wall functions provided that the first grid point has $y^+ \approx 1$ near the wall[25]. On the other hand, the model depends on the global minimum wall distance and cannot accurately predict the unsteady features of vortex breakdown and massively separated flows.

It has been shown that eddy-viscosity-based models improve mean flow predictions if an empirical rotation and streamline curvature correction is incorporated[23]. Spalart and Shur[26]

https://doi.org/10.1017/S0001924000010575 Published online by Cambridge University Press

modified the original SA turbulence model with Rotation and Curvature correction. In the SARC model, the production term in the eddy viscosity transport equation is multiplied by the rotation function given by;

$$P = C_{b1}(f_{r1} - f_{t2})W\tilde{v} \quad \ldots (4)$$

where f_{rl} is the rotation correction factor. The SARC model has been widely used for aerodynamic prediction of aircraft with vortical flows.

Although, RANS models remain popular, hybrid RANS/LES (large-eddy simulation) models are still required for predicting unsteady separated flows. One hybrid RANS/LES approach is the Delayed Detached-Eddy Simulation (DDES) model originally proposed by Spalart *et al*[27]. In this model, the SA model is applied to the boundary-layer region and LES is used for the separated regions. The approach is substantially less costly than LES, while it can achieve better accuracy than the SA model for predicting separated flows[28]. DDES models have been use with other turbulence models as well. These models largely depend on the grid spacing and the prediction of the boundary layer.

2.4 Vortical flows

The vortical flow behavior over delta wings is extremely complex and differs substantially from nonslender to slender wings. These vortices have been extensively studied experimentally and computationally over the past two decades[29,30,31]. In a slender wing, the flow at high angles of attack is characterised by two large counter-rotating primary vortices formed over the upper surface. The sharp leading edges of slender wings cause the boundary layer to separate and the separated shear layers to roll up into vortices[31]. The shear layer may exhibit instabilities that increase the vortical substructures and, therefore, the primary vortex increases in both size and strength as it extends

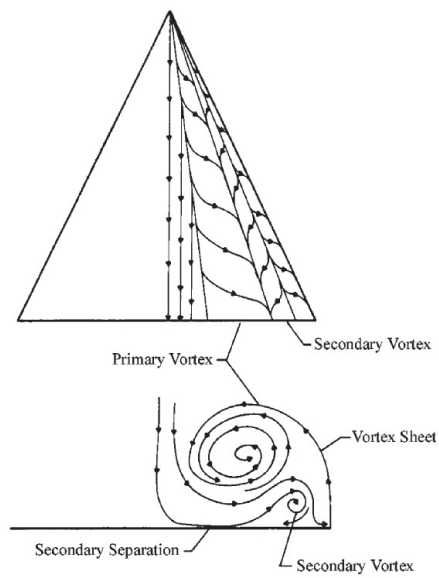


Figure 2. Primary and secondary vortices above a slender wing[4].

https://doi.org/10.1017/S0001924000010575 Published online by Cambridge University Press

downstream. Each vortex core is approximately one core diametre above the lifting surface of the wing[32]. It has been shown that the interaction of the primary vortices with the surface boundary layer can cause the boundary layer to separate and roll up to form smaller secondary vortices of the opposite sign of vorticity of the primary vortex as shown in Fig. 2. Over a nonslender wing, the vortices are formed much closer to the surface of the wing than those over slender wings. The interaction of the secondary vortices with the shear layer of the primary vortex causes the primary vortex to split into a dual primary vortex structure[32]. Since the cores of vortices over nonslender wing are much closer to the surface and its boundary layer, the flow over nonslender wings is more sensitive to Reynolds number than flows over slender wings[32].

The leading-edge vortices have significant effects on the aerodynamic behavior of aircraft; they form regions of high vorticity and low-pressure over the upper wing surface that cause a nonlinear increase in lift until the maximum attainable lift with attached flow[29]. At high angles of attack, the vortex structures change dramatically, leading to vortex breakdown, which is known to cause non-linear aerodynamic behavior. Vortex breakdown is characterised by a sudden deceleration of the axial flow in the vortex core, a decrease in circumferential velocity, and an increase in vortex size and turbulent dissipation[2]. The onset of vortex breakdown starts from the trailing-edge of the wing and moves forward on the wing with increasing angle-of-attack until, at sufficiently high angle-of-attack, the flow is dominated by the periodic wake shedding encountered over bluff bodies[33]. Note that a slender wing attains its maximum lift and stalls approximately when the onset of vortex breakdown crosses the trailing edge, while wings with smaller sweep angles stall when the onset of vortex breakdown moves towards the wing apex[2].

3.0 TEST CASE

The X-31 aircraft is considered in this work. The aircraft geometry and wind-tunnel data were provided to the participants in NATO RTO Task Group AVT-161 (Assessment of Stability and Control prediction Methods for NATO Air and Sea Vehicles)[34]. The objective of this task group is to evaluate CFD codes against wind-tunnel results. A three-view drawing of the vehicle is shown in

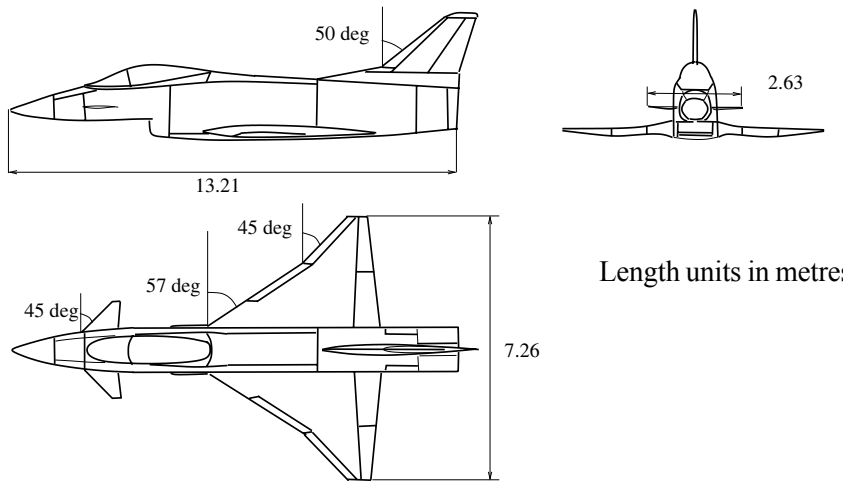


Figure 3. X-31 aircraft geometry.

https://doi.org/10.1017/S0001924000010575 Published online by Cambridge University Press

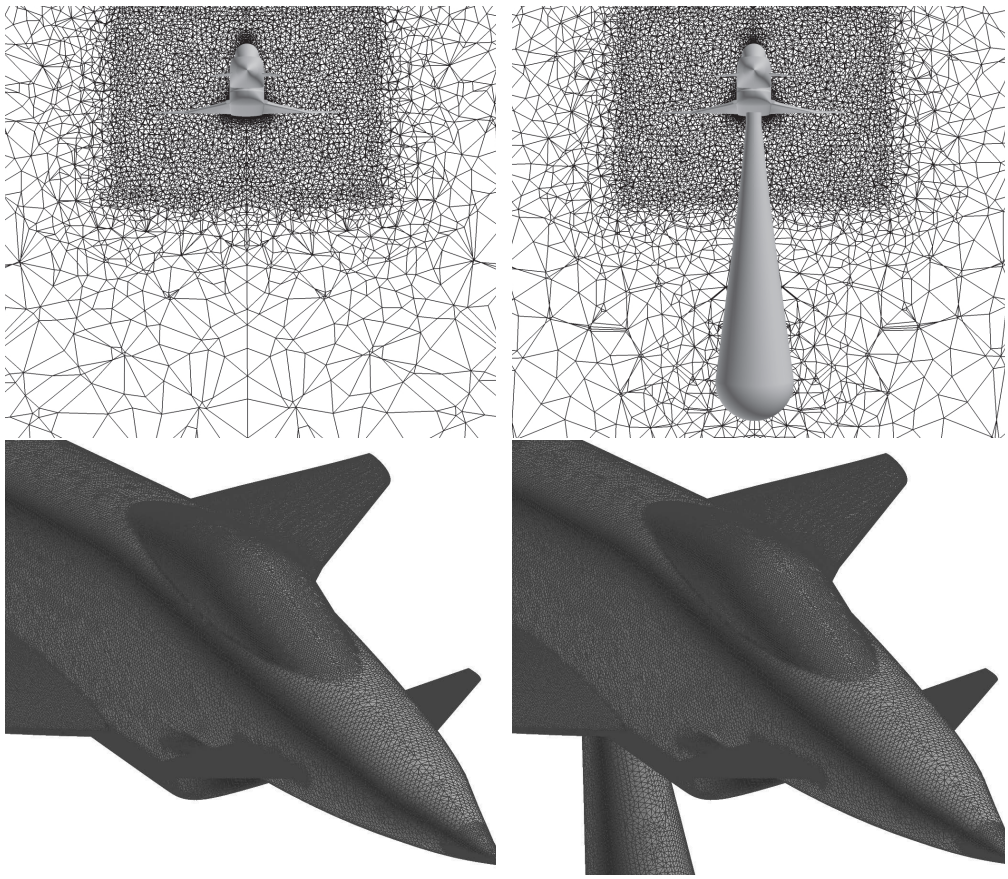
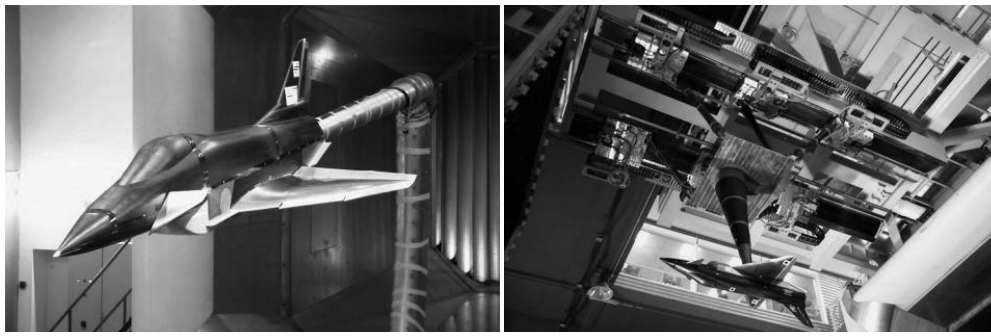


Figure 4. X-31 aircraft mesches.

Fig. 3. The aircraft has a fuselage length of 13·21m, a canard, and a double delta wing with a total wing span of 7·26m. The inner delta wing has a sweep angle of 57° and the outer sweep is 45°. The inner wing sweep places the wing behind the supersonic shock wave, while the outer sweep improves the vehicle stability and control[35]. The canard is a cropped delta wing with a sweep angle of 45°. Additional characteristics of aircraft are the inner and outer leading edge flaps, the trailing-edge flaps, the front wing and rear fuselage strakes. The moving surfaces include canard, inner and outer slats, flaps, rudder, and thrust vector paddles.

The wind-tunnel models have a wing span of one metre, therefore they are 1/7·26 smaller than the actual aircraft. Note that control surfaces and gaps between them are not modeled in these studies. Two meshes are available, corresponding to X-31 wind-tunnel models with and without a belly mounted sting. The RANS meshes were generated in two steps. In the first step, the inviscid tetrahedral mesh was generated from a clean configuration using the ICEM-CFD code. The inviscid mesh was then used as a background mesh by TRITET[26] which builds prism layers using a frontal technique. TRITET rebuilds the inviscid mesh while respecting the size of the original inviscid mesh from ICEM-CFD. Mesh overviews are shown in Fig. 4. Both grids are symmetric configurations. The grid without the sting contains 4·9 million points and 11·7 million

https://doi.org/10.1017/S0001924000010575 Published online by Cambridge University Press



(a) X-31 model on the $\alpha - \beta$ sweep support (b) X-31 model on the MPM

Figure 5. X-31 wind-tunnel models in DNW-NWB Braunschweig[11].

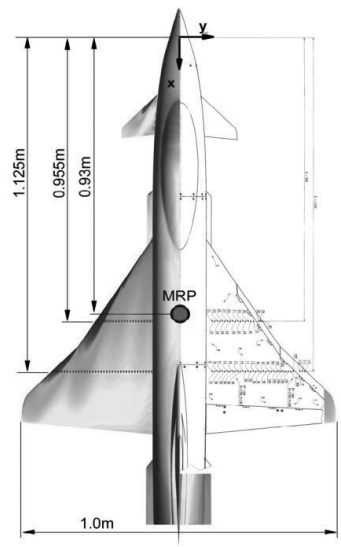


Figure 6. Wind tunnel model surface pressure measurement locations[11]; MRP – moment reference point.

cells, and the grid with the sting contains 5·5 million points and 12·9 million cells. Note that the forces and moments acting on the sting are not included in the total aircraft airload calculations.

4.0 WIND-TUNNEL EXPERIMENTS

The X-31 wind-tunnel data are available from the German-Dutch Low-Speed Wind-tunnel facility in Braunschweig (DNW-NWB), Germany, which is an atmospheric wind tunnel of closed-circuit type and has a test section size of 2·8 × 3·25 m with a maximum free stream velocity of 90ms^{-1}[38]. The tunnel is capable of conducting static and dynamic measurements using different support systems; it can measure static forces and moments up to high angles of attack using a rear sting support in the $\alpha - \beta$ sweep configuration and can perform dynamic motions using the Model Positioning Mechanism (MPM) with a belly mounted support as shown in Fig. 5. Other available support systems are half-model setup, two-dimensional testing setup, and rotary motion support.

https://doi.org/10.1017/S0001924000010575 Published online by Cambridge University Press

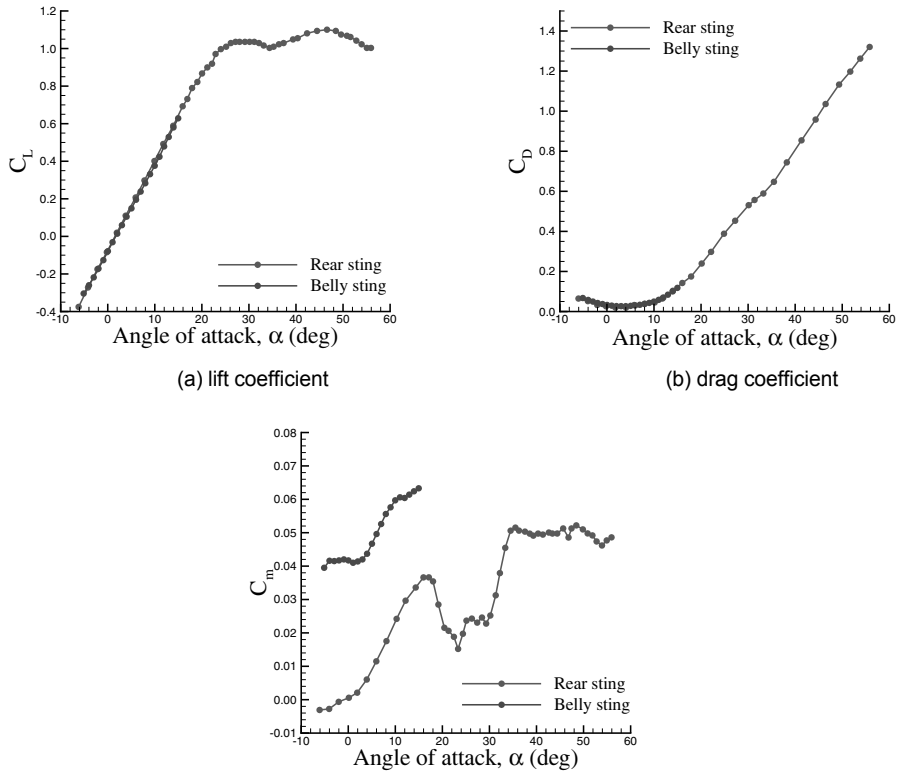


Figure 7. X-31 experimental data from the $\alpha = \beta$ sweep and MPM supports.

The X-31 wind-tunnel models includes all actual aircraft control surfaces; these surfaces can be remote controlled or manually adjusted. Static measurements were reported from $\alpha - \beta$ sweep and MPM supports (supports with rear sting and belly mounted sting, respectively), while the belly-mounted configuration data are limited to +15 degrees angle-of-attack only. Data were reported for two X-31 geometries; one with open gaps at the wing trailing-edge flaps and the other with sealed gaps. The data of the sealed-gap model are used here. Note that the gaps between the leading-edge flaps and wing are not sealed in the experiments. The X-31 wind-tunnel model has a wing span of one metre, a reference area (wing area) of 0·3984m^2, mean aerodynamic chord of 0·51818 metre, and a moment reference point (MRP) of (0·93,0,0) metre. The belly-mounted sting has a length of around 1·6m. Forces and moments were measured with an internal six component strain gauge balance[38]. The surface pressure distribution was measured by two spanwise pressure tap rows at locations of 60% and 70% chord length, as shown in Fig. 6.

5. RESULTS AND DISCUSSION

All CFD simulations were run on the Cray XE6 machine at the Engineering Research Development Center (ERDC); the machine name is Garnet and has near 150,000 processors and a 2·7GHz core speed.

https://doi.org/10.1017/S0001924000010575 Published online by Cambridge University Press

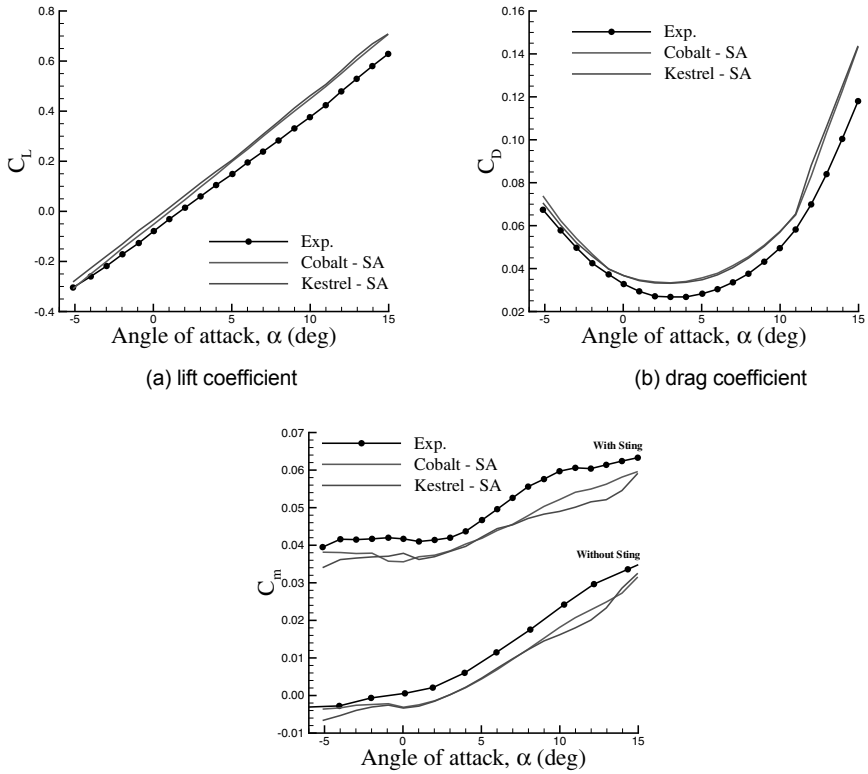


Figure 8. Validation of Cobalt and Kestrel simulations using the SA turbulence model.

Two experimental data sets were selected from X-31 measurements in the DNW-NWB: test runs VN01004 and VN1002 which use a rear sting and a belly-mounted sting, respectively. The angles of attack in VN01004 range from –6 to 55 with zero side-slip angle and zero control surface deflections. The second data set covers the –5 to 15 angle-of-attack range, again with zero side-slip angle and zero control surface deflections. In both experiments, the wind-tunnel speed was 60ms^{-1} with a chord-based Reynolds number of 2·063. The wind-tunnel models in both experiments have open gaps between leading edge flaps as shown in Fig. 6, but these gaps are not included in the computational grids. Figure 7 shows the measured values of lift, drag, and pitch moment from the VN01004 and VN1002 test runs.

The results of the comparison show that the lift coefficients are slightly higher for the VN01004 test run with the rear sting, but the pitch moment values of this test run are substantially smaller than the VN1002 measured pitch moments. Also, the pitch moment slopes in both experiments are different; the rear sting model predicts a positive slope at zero angles of attack, but the belly-mounted model shows a negative slope at this angle. These experiments show that the presence of the belly-mounted sting changes the aerodynamic characteristics of the model and increases the integrated pitch moment. Note that the slopes of the pitch moment curves are small, representing the fact that the moment reference point is close to the aircraft neutral point. Therefore, a small change in the flow can have significant effects on the pitch moment slope. For example, Fig. 7

https://doi.org/10.1017/S0001924000010575 Published online by Cambridge University Press

shows that at 18° angle-of-attack, the X-31 model has not yet stalled, but the pitch moment falls rapidly at this angle because of the presence of wing vortex breakdown at the wing trailing edge. The movement of the vortex breakdown position with further increases in angle-of-attack makes the pitch moment behavior very nonlinear as shown in Fig. 7 (c).

Cobalt and Kestrel simulations using the SA turbulence model are compared with experimental data in Fig. 8. These simulations cover the –5° to 15° angle-of-attack range. A first-order accuracy in time was used and the simulations were iterated in time until a converged solution was reached. The use of first order in time model was justified because no vortex breakdown was observed over the range of angles of attack considered. The oscillations in the forces and moments are smaller than the steady state values. The main source of unsteadiness in the flow is the wake behind the belly-mounted sting. However, the sting forces and moments were not included in the aircraft predictions. The flow input conditions correspond to that of the experimental data. The exact experimental angles of attack were used in the CFD, allowing the comparison of surface pressure predictions with measurements. The total run time of the model with the sting is near three hours using 512 processors for each angle-of-attack (the runtime of the model without the sting is a little less). Figure 8 shows that Kestrel and Cobalt overestimate experimental lift coefficients. Differences between CFD and the measured lift become larger if the angle-of-attack increases. Discrepancies can also be seen in the drag and pitch moment comparison plots, especially at high angles of attack. These differences are most likely due to the presence of the open gaps around the leading flaps in the wind-tunnel models. This will be discussed in more detail below.

In general, a good match between Cobalt and Kestrel predictions was found. Again, it should be noted that the moment reference point is close to the aircraft neutral point, and therefore pitch moment values are sensitive to the differences in the numerical algorithms of the solvers. Thus pitch moments from Cobalt and Kestrel do not match everywhere, however, these differences are small. Figure 8 shows that both solvers correctly predict the flow structures and their effects on the forces and moments; for example CFD predictions accurately predict the offset seen in the experimental pitch moment due to the wake formed behind the belly mounted sting. This wake is formed even at small angles of attack as shown in Fig. 9, that shows the predicted wake from Cobalt at zero degrees angle-of-attack. The wake region is highlighted by eddy viscosity ratio iso-surfaces

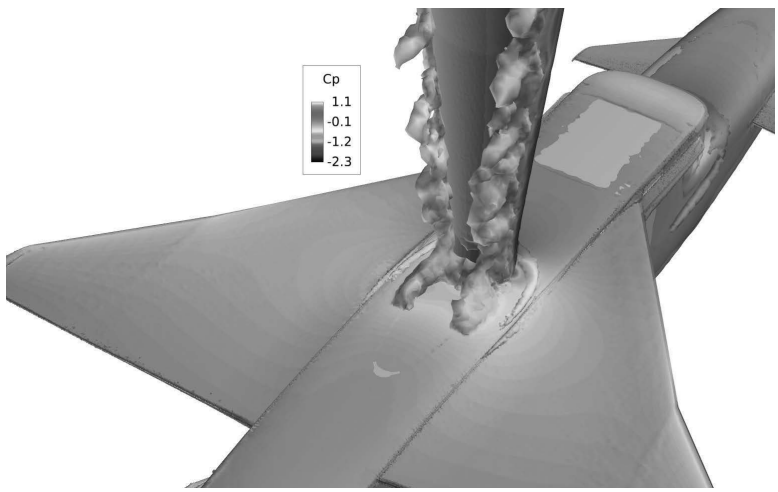


Figure 9. The wake behind belly sting predicted by Cobalt using the SA turbulence model. Angle-of-attack is zero degrees.

https://doi.org/10.1017/S0001924000010575 Published online by Cambridge University Press

coloured by pressure coefficients. Figure 10 shows that the wake behind the sting affects the flow on the lower side of the wing; there is a high pressure region formed in front of the sting and a low pressure region formed behind the sting which stretches towards the wing tip. The moment reference point is located at the centre of the sting. The formation of a large region of small pressure flow behind the sting (and therefore behind the moment reference point) causes the aircraft to pitch up (a positive pitch moment). The wake effects on the pitch moment depend on the angle-of-attack, such that it has less offset in pitch moment values at higher angles for the range of angles studied.

The experimental surface pressure distributions are available from spanwise taps at 60% and 70% chord length. The co-ordinates of these taps were input to the Cobalt and Kestrel solvers. The codes then write the calculated flow parametres (selected by the user) at these locations. The files can be written at each iteration or report the time-averaged values from selected iterations. In this work, the pressure coefficients from the final iteration are used. These results are compared with measurements at different angles of attack and are shown in Fig. 11.

Each figure shows two set of lines at each experimental location corresponding to two spanwise stations on the wing. The 70% chord length has more spanwise locations due to the swept of the wing. Fig. 11(a) shows that at almost all locations, Cobalt and Kestrel predictions at –5·12° angle-of-attack match well with experiments. At this angle, the pressure coefficients at the upper surface near the wing tip are positive. At zero degrees angle-of-attack, the pressure coefficients become smaller as shown in Fig. 11 (b), although CFD and experimental data still match well everywhere.

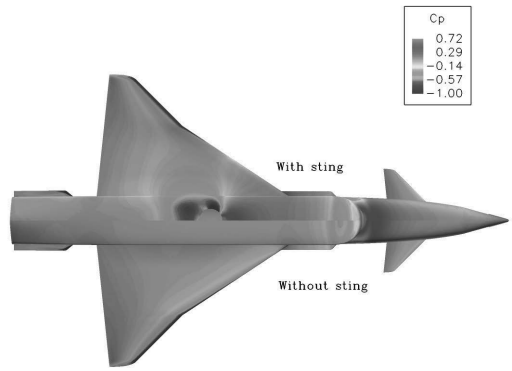
At an angle-of-attack of 5°, the pressure coefficients are negative and decrease from the fuselage towards the wing tip due to the wing sweep angle as shown in Fig. 11 (c). A small dip can be seen in pressure data at the –111mm span location; this is caused by the LEX vortex effects on the upper wing. Figure 11 (c) shows that the CFD calculations predict the trends correctly and match measurements quite well. The biggest discrepancies appear at spanwise locations close to the wing tip where the open flap gaps are present. At these locations, the CFD solvers predict more negative pressure coefficients than the measurements.

Figure 11 (d) shows that the pressure coefficients become more negative at an angle-of-attack of 11°; CFD and experimental data still match everywhere except at the wing tip. At an angle-of-attack of 13°, a wing vortex is formed which causes a sudden dip in pressure coefficient data at 60% chord as shown in Fig. 11 (e). The wing vortex produces negative pressure values, where the minimum value occurs in the vortex core. Cobalt and Kestrel predicted the dip but the vortex spanwise locations are slightly off. For data at 70% chord, the wing vortex also causes a dip in the pressure data (the minimum value is around –300mm). However, the pressure changes are much smaller than those seen in 60% chord. As the vortex stretches over the wing, it becomes bigger in size and has less negative pressure values due to adverse pressure gradients. Cobalt and Kestrel predict the vortex flow structures, but they predict a stronger vortex than experiments.

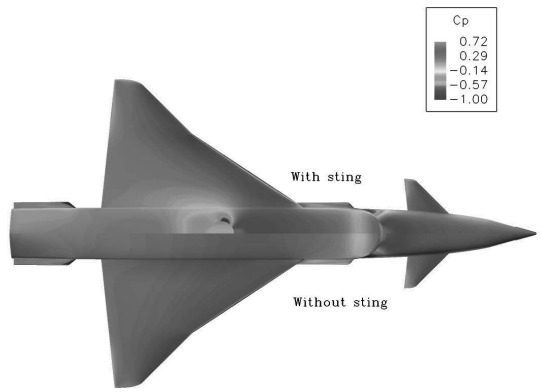
There is also a large difference between CFD and experiments for spanwise taps located above the –350mm location. At high angles of attack, experiments show another vortex flow due to the open gap flaps which causes another dip in the pressure data. However, CFD predictions do not show this vortex and its effects due to having sealed gaps in the CFD geometries. At an angle-of-attack of 15°, the wing vortex becomes stronger and larger and shows more negative pressure values as shown in Fig. 11(f). The flap vortex becomes stronger as well, but it cannot be seen in the CFD solutions.

The wing and LEX vortices from Cobalt can be seen in Fig. 12 for an angle-of-attack of 15°. The planes in this figure are created at 60% and 70% chord lengths, and show the flow vorticity. Figure 12 shows that the pressure coefficient is small but vorticity is large at the vortex cores; the wing vortex core has less negative pressure values than pressures calculated at the LEX vortex

https://doi.org/10.1017/S0001924000010575 Published online by Cambridge University Press



(a) α = 0·03°



(b) α = 14·97°

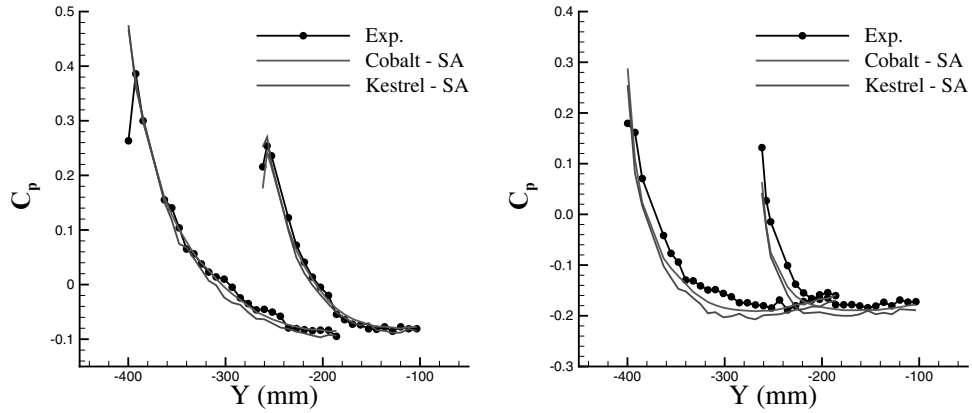
Figure 10. Effects of sting on the surface pressure solutions.
Simulations are from Cobalt using SA turbulence model.

core. There is also a region of high pressure between the two vortices. This region can be seen with a nearly constant pressure line in Figs. 11(e)-(f). At 70% chord length, both vortices are bigger in size and have higher pressures than 60% chord length due to adverse pressure gradients.

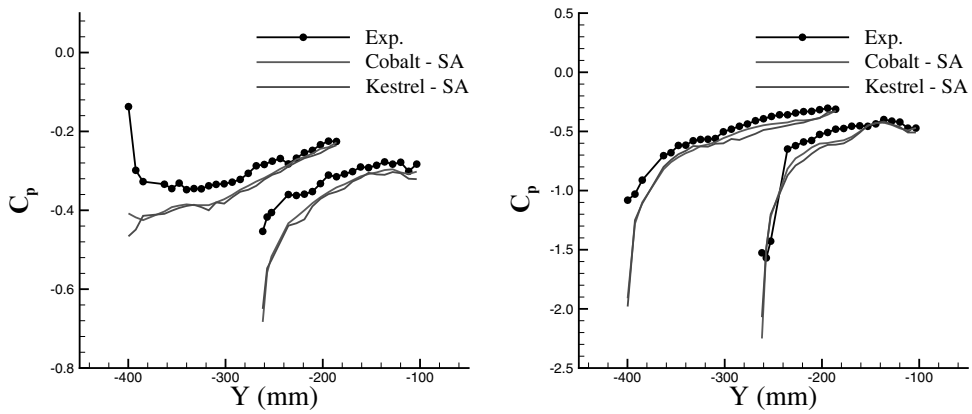
Figure 13 shows the flow solutions from Cobalt and Kestrel at different angles of attack. In general, the predictions from both codes are quite close, especially at low angles of attack. Figure 13 (d) shows that at 15 degrees angle-of-attack, there are canard, LEX, and wing vortices. At this angle, the vortices predicted from Cobalt and Kestrel are shown in Fig. 14; Kestrel predicts stronger vortices than Cobalt.

Figures 15 and 16 show the effects of the SARC turbulence modeling on the predictions. The results show that SARC overestimates lift data compared to the SA model; the drag predictions of low angles of attack match better with experiments, but they overestimate experimental drag at higher angles. Cobalt pitch moment values at low angles of attack are better using SARC. With respect to the pressure data, SARC slightly underestimates SA data for low angles of attack. At angle-of-attack, SARC predicts the wing vortex where SA and experiments do not show it. At higher angles of attack, SARC predicts a stronger wing vortex in both codes. In general, SARC predictions did not improve the CFD solutions much at these angles of attack. Over the range of these angles of attack, no vortex breakdown was detected.

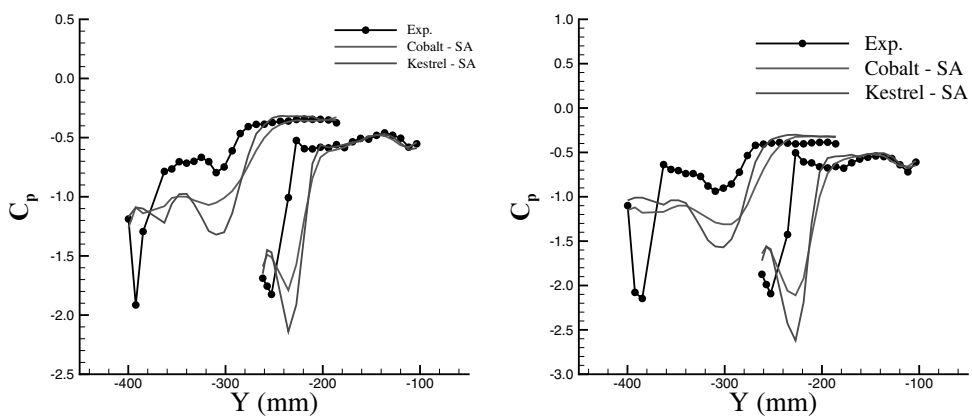
https://doi.org/10.1017/S0001924000010575 Published online by Cambridge University Press



(a) α = –5·12° (b) α = 0·03°



(c) α = 5·04° (d) α = 10·99°



(e) α = 12·96° (f) α = 14·97°

Figure 11. Validation of Cobalt and Kestrel surface pressure coefficients using SA turbulence model.

https://doi.org/10.1017/S0001924000010575 Published online by Cambridge University Press

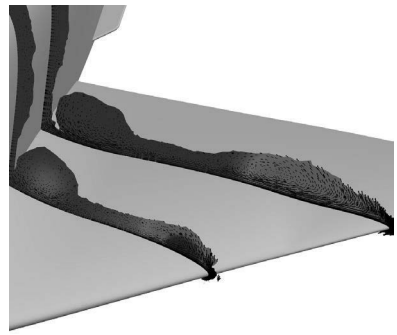


Figure 12. Cobalt-SA surface pressures at two tap locations. Angle-of-attack is 14·97 degrees.

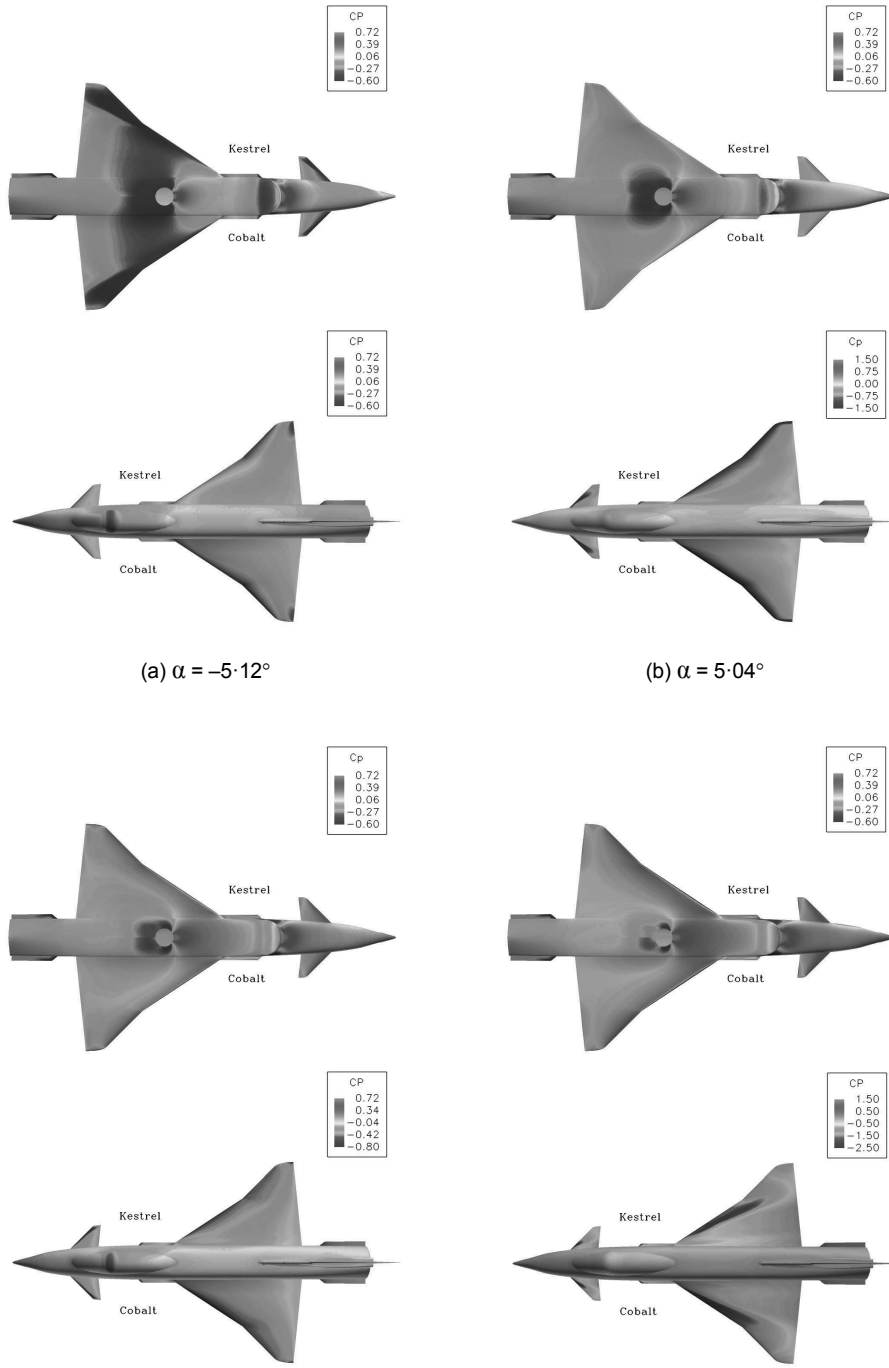
Figure 17 compares the lift, drag, and pitch moment coefficients obtained from Cobalt using DDES with SARC, SA, and SARC with wind tunnel data using the rear sting support. These simulations use second-order accuracy in time with three Newton subiterations and 3,000 time steps. Figure 17 shows that all these models yield similar predictions at low angles of attack, but they result in a wide spread of predictions at moderate to high angles. For angles above $\alpha = 18°$, SARC-DDES and SARC models perform quite well compared with SA. The DDES is even more accurate than SARC for accurately predicting unsteady separated flows occurring at these angles. For higher angles of attack, DDES simulations should run for more iterations and time-averaging the solutions should be considered.

6.0 CONCLUSIONS

This paper focused on the validation results of X-31 wind-tunnel models using the Cobalt and Kestrel flow solvers. The predictions were compared with the DNW-NWB experimental data at low speeds and $Re = 2{\cdot}063 \times 10^6$ for wind-tunnel models with rear and belly-mounted sting supports. These experiments showed that the X-31 pitching moment is a strong nonlinear function of angle-of-attack and its value and slope changes with the presence of a belly-mounted sting. Previous work showed that high angle-of-attack flow around the X-31 is very unsteady due to canard, LEX, and wing vortex breakdown. These features make the validation of CFD solvers a challenging task. The computational grids are RANS meshes which were generated from X-31 wind-tunnel geometries with and without a belly-mounted sting. In these meshes, the gaps between leading-edge flaps and wings were sealed. The moment reference point was set to a point close to the wind-tunnel model neutral point. The simulations were obtained using SA, SARC, and DDES with SARC turbulence models.

The results showed that Cobalt and Kestrel solutions are similar and match quiet well with experiments for small to moderate angles of attack. The main discrepancies between CFD and measurements occur close to the wing tip, where leading edge flaps are placed. CFD pressure distributions show more negative pressures at this region than measurements. At high angles of attack, the differences become larger because of flap vortex formation, but the CFD solvers did not predict this vortex due to sealed gaps in the geometries. Apart from this discrepancy, both Cobalt and Kestrel predict the effects of wing and LEX vortices on surface pressure. The CFD solutions showed that the wake behind the sting affects the flow at the lower side of the wing, causing the aircraft to pitch up (a positive pitch moment) as observed in the experiments. CFD solutions using SARC showed stronger vortices formed than SA, even predicting the wing vortex at smaller angles of attack. The SARC solutions did not improve predictions much until an angle-of-attack at which vortex breakdown

https://doi.org/10.1017/S0001924000010575 Published online by Cambridge University Press



(a) $\alpha = -5{\cdot}12°$ (b) $\alpha = 5{\cdot}04°$

(c) $\alpha = 10{\cdot}99°$ (d) $\alpha = 14{\cdot}97°$

Figure 13. Cobalt and Kestrel surface pressure solutions using SA turbulence model.

https://doi.org/10.1017/S0001924000010575 Published online by Cambridge University Press

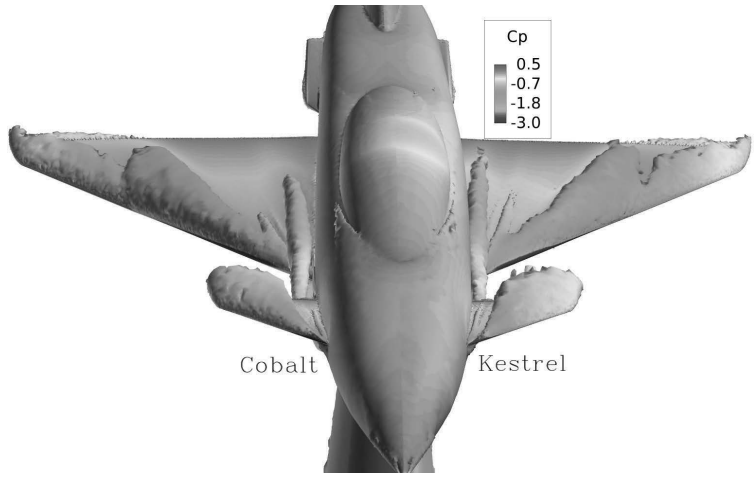
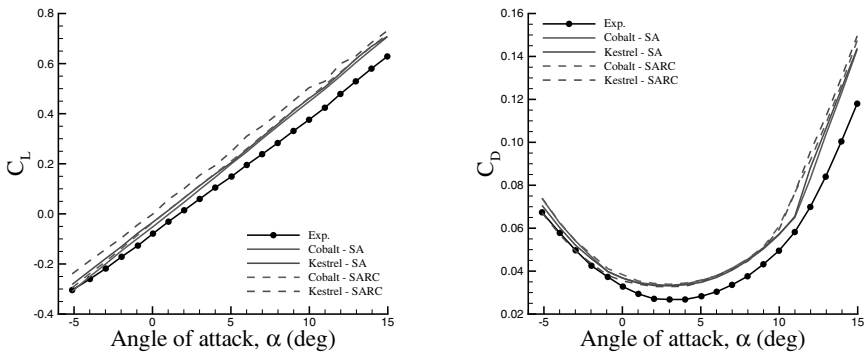
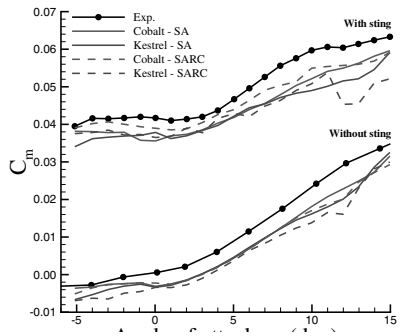


Figure 14. X-31 predicted vortical flows of Cobalt and Kestrel solvers with SA turbulence model at α = 14·97°.



(a) lift coefficient

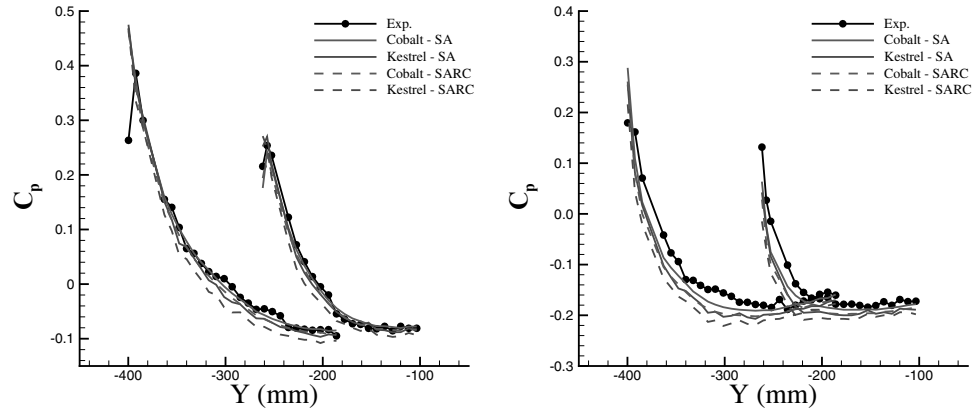
(b) drag coefficient



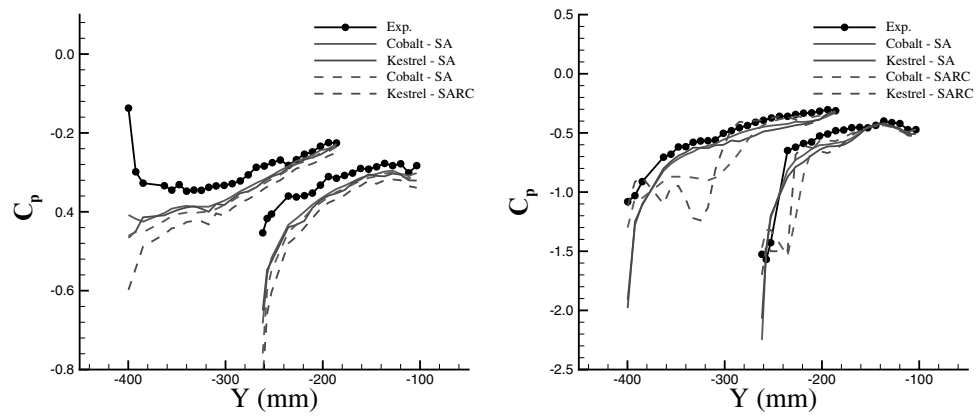
(c) pitching moment coefficient

Figure 15. Validation of Cobalt and Kestrel simulations using the SARC turbulence model. Experiments correspond to VN1002 test run with MPM support.

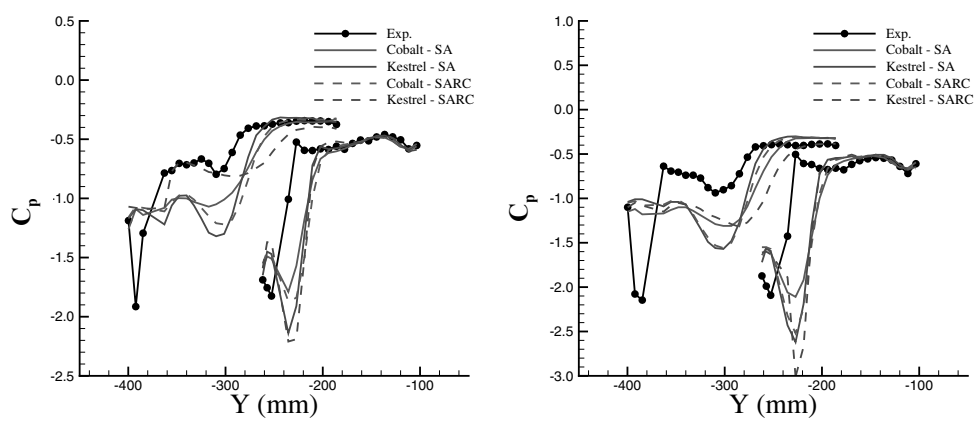
https://doi.org/10.1017/S0001924000010575 Published online by Cambridge University Press



(a) α = –5·12° (b) α = 0·03°



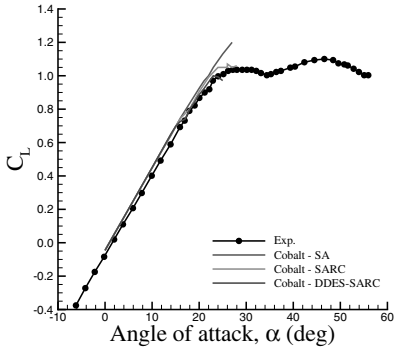
(c) α = 5·04° (d) α = 10·99°



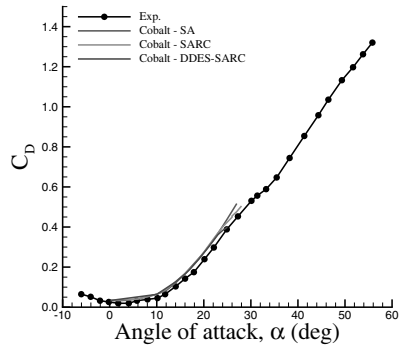
(e) α = 12·96° (f) α = 14·97°

Figure 16. Validation of Cobalt and Kestrel surface pressure coefficients using the SARC turbulence model.

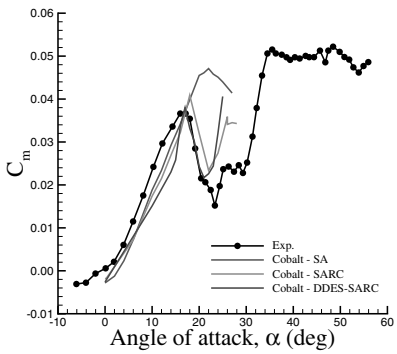
https://doi.org/10.1017/S0001924000010575 Published online by Cambridge University Press



(a) lift coefficient



(b) drag coefficient



(c) pitching moment coefficient

Figure 17. Validation of Cobalt simulations for the model using $\alpha = \beta$ sweep support.

occurs. At and beyond this angle-of-attack, the SA model fails to predict the vortex breakdown and its effects due to the diffusive nature of the model. Adding the rotation correction in SARC helps to predict the vortex breakdown effects, although the CFD data were slightly off. The results show that DDES-SARC model has the best accuracy of predicting the flow around X-31 at high angles of attack.

Future work will extend the results to include validation of dynamic motions and simulations using other turbulence models. A new grid will be generated that has the open gaps present in the wind-tunnel models to investigate the effects of the vortex due to flaps.

ACKNOWLEDGEMENTS

Mehdi Ghoreyshi is supported by USAFA under contract FA70001320018; their financial support is gratefully acknowledged. Computer time was provided by the Department of Defense Engineering Research Development Center (ERDC). The X-31 geometry was provided by NATO RTO Task Group AVT-161 on assessment of stability and control prediction methods for NATO air and sea vehicles. The authors appreciate the support provided by the High Performance Computing Research Center and Col Robert Kraus, USAFA Chief Scientist. The authors would also like to thank Andreas Schütte of DLR and Okko Boelens of NLR for providing X-31 experimental data.

https://doi.org/10.1017/S0001924000010575 Published online by Cambridge University Press

REFERENCES

1. CUMMINGS, R.M. Update on computational aerodynamics education at the US Air Force Academy, *Int J Aerodynamics*, 2012, **2**, (1), pp 93-109.
2. PAMADI, B.N. Performance, Stability, Dynamics, and Control of Airplanes, AIAA Education Series, AIAA, Reston, Virginia, USA, 2004.
3. TU, E.L. Effects of canard deflection on close-coupled canard-wing-body aerodynamics, *J Aircr*, 1994, **31**, (1), pp 138-145
4. NELSON, R.C. and PELLETIER, A. The unsteady aerodynamics of slender wings and aircraft undergoing large amplitude maneuvers, *Progress in Aerospace Sciences*, 2003, **39**, (2), pp 185–284.
5. REIN, M., HÖHLER, G., SCHÜTTE, A., BERGMANN, A. and LÖSER, T. Ground-Based Simulation of Complex Maneuvers of a Delta-Wing Aircraft, AIAA Paper 2006–3149, June 2006.
6. STRANG, W.Z., TOMARO, R.F. and GRISMER, M.J. The defining methods of cobalt: a parallel, implicit, unstructured Euler/Navier-Stokes flow solver, AIAA Paper 1999–0786, January 1999.
7. MORTON, S.A., MCDANIEL, D.R., SEARS, D.R., TILLMAN B. and TUCKEY, T.R. Kestrel: a fixed wing virtual aircraft product of the CREATE program. AIAA Paper 2009-0338, January 2009.
8. GOTTLIEB, J.J. and GROTH, C.P.T. Assessment of Riemann solvers for unsteady one-dimensional inviscid flows of perfect gasses, *J of Computational Physics*, 1988, **78**, (2), pp 437–458.
9. GODUNOV, S.K. A difference scheme for numerical computation of discontinuous solution of hydrodynamic equations, *Sbornik Mathematics*, 1959, **47**, pp 271-306.
10. SCHÜTTE, A., EINARSSON, G., RAICHLE, A., SCHONING, B., MÖNNICH, W. and FORKERT, T., Numerical simulation of manoeuvreing aircraft by aerodynamic, flight mechanics, and structural mechanics coupling, *J Airc*, 2009, **46**, (1), pp 53–64.
11. SCHÜTTE, A., BOELENS, O.J., LÖSER, T. and OEHLKE, M. Prediction of the Flow around the X-31 aircraft using two different CFD methods, AIAA Paper 2010-4692, June-July 2010.
12. BOELENS, O.J. CFD Analysis of the flow around the X-31 aircraft at high angle-of-attack, AIAA Paper 2009-3628, June 2009.
13. ANTON, N. and BOTEZ, R.M. Aircraft X-31 stability analysis and validation with experimental data. Proceedings of the IASTED International Conference on Applied Simulation and Modeling, 25-27 June 2012, Naples, Italy, pp 114-118, Calgary, Acta Press.
14. ANTON, N., BOTEZ, R.M. and POPESCU, D. Stability derivatives for a delta-wing X-31 aircraft validated using wind tunnel test data, *J Aerospace Engineering*, 2011, **225**, pp 403-416.
15. ALCON, C.W., CROOM, M.A. and FRANCIS, M.S. The X-31 Experience – Aerodynamic impediments to post-stall agility, AIAA Paper 1995–362, January 1995.
16. WILLIAMS, D.L., NELSON, R.C. and FISHER, D. An Investigation of X-31 roll characteristics at high angle-of-attack through subscale model testing, AIAA Paper 1994–806, January 1994.
17. TOMARO, R.F., STRANG, W.Z. and SANKAR, L.N. An implicit algorithm for solving time dependent flows on unstructured grids, AIAA Paper 1997–0333, January 1997.
18. SPALART, P.R. and ALLMARAS, S.R.A. One equation turbulence model for aerodynamic flows. AIAA Paper 1992-0439, January 1992.
19. WILCOX, D.C. Reassesment of the scale determining equation for advanced turbulence models, *AIAA J*, 1988, **26**, pp 1299-1310.
20. MENTER, F. Eddy viscosity transport equations and their relation to the model, *ASME Journal of Fluids Engineering*, 1997, **119**, pp 876-884.
21. ROTH, G.L., MORTON, S.A. and BROOKS, G.P. Integrating CREATE-AV products DaVinci and Kestrel: experiences and lessons learned. AIAA Paper 2012-1063, January 2012.
22. GRISMER, M.J., STRANG, W.Z., TOMARO, R.F. and WITZMMAN, F.C. Cobalt: a parallel, implicit, unstructured Euler/Navier-stokes solver, *Advanced Engineering Software*, 1998, **29**, (3-6), pp 365-373.
23. CHURCHFIELD, M.J. and BLAISDELL, G.A. Reynolds stress relaxation turbulence modeling applied to a wingtip vortex flow, *AIAA J*, 2013, **51**, (11), pp 2643-2655.
24. SWANSON, R.C. and RUMSEY, C.L. Numerical issues for circulation control calculations, AIAA Paper 2008-3008, June 2008.
25. BIGARELLA, E. and AZEVEDO, J. Advanced eddy-viscosity and Reynolds-stress turbulence model simulations of aerospace applications, *AIAA J*, 2007, **45**, (10), pp 2369-2390.
26. SPALART, P.R. and SHUR M.L. On the sensitization of turbulence models to rotation and curvature, *Aerospace Science Technology*, 1997, **1**, pp 297–302.

https://doi.org/10.1017/S0001924000010575 Published online by Cambridge University Press

27. SPALART, P.R., JOU, W.-H., STRELETS, M. and ALLMARAS, S.R. Comments on the Feasibility of LES for Wings, and on a Hybrid RANS/LES Approach. In Proceedings, 1st AFSOR International Conference on DNS/LES, Greyden Press, Columbus, Ohio, USA, 1997, pp 137–147.
28. TRAPIER, S., DECK, S. and DUVEAU, P. Delayed detached-eddy simulation and analysis of supersonic inlet buzz, *AIAA J*, 2008, **46**, (1), pp 118-131.
29. THOMAS, J.L., KRIST, S.T. and ANDERSON, W.K. Navier-Stokes computations of vortical flows over low-aspect-ratio wings, 1990, *AIAA J*, **28**, (2), pp 205-212.
30. GURUL, I., GORDNIER, R. and VISBAL, M. Unsteady aerodynamics of nonslender delta wings, *Progress in Aerospace Sciences*, 2005, **41**, pp 515–557.
31. VALLESPIN, D., DARONCH, A., BADCOK K.J. and BOELENS, O.J. Vortical flow prediction validation for an unmanned combat air vehicle model, *J Aircr*, 2011, **48**, (6), pp 1948-1959.
32. TAYLOR, G.S., SCHNORBUS, T. and GURSUL, I. An investigation of vortex flows over low speed delta wings. AIAA Paper 2003-4021, June 2003.
33. CUMMINGS, R.M., FORSYTHE, J.R., MORTON, S.A. and SQUIRES, K.D. Challenges in high angle-of-attack flow prediction, *Progress in Aerospace Sciences*, 2003, **39**, (5), pp 369-384.
34. CUMMINGS, R.M. and SCHÜTTE, A. An integrated computational/experimental approach to UCAV stability & control estimation: overview of NATO RTO AVT-161, AIAA Paper 2010–4392, June-July 2010.
35. SCHEFTER, J. X-31: How They´re inventing a radical new way to fly, *Popular Science*, 1989, **234**, (2), pp 58–64.
36. TYSSEL, L. Hybrid grid generation for complex 3D geometries, Proceedings of the 7th International Conference on Numerical Grid Generation in Computational Field Simulation, 2000, pp 337–346.
37. TYSSEL, L. The TRITET grid generation system, International Society of Grid Generation (ISGG), Proceedings of the 10the International Conference on Numerical Grid Generation in Computational Field Simulations, 2000.
38. LÖSER, T. and BERGMANN, A. Develop of the dynamic wind tunnel testing capabilities at DNW-NWB. AIAA Paper 2003-453, January 2003.

https://doi.org/10.1017/S0001924000010575 Published online by Cambridge University Press